Accepted Manuscript

New insight into the allosteric effect of L-tyrosine on mushroom tyrosinase during L-dopa production

Sorour Hassani, Behzad Gharechaei, Somayeh Nikfard, Mostafa Fazli, Nematollah Gheibi, Renaud Hardré, Raymond L. Legge, Kamahldin Haghbeen

PII: S0141-8130(18)30754-2
DOI: doi:10.1016/j.ijbiomac.2018.03.185
Reference: BIOMAC 9407

To appear in:

Received date: 14 February 2018
Revised date: 30 March 2018
Accepted date: 31 March 2018

Please cite this article as: Sorour Hassani, Behzad Gharechaei, Somayeh Nikfard, Mostafa Fazli, Nematollah Gheibi, Renaud Hardré, Raymond L. Legge, Kamahldin Haghbeen , New insight into the allosteric effect of L-tyrosine on mushroom tyrosinase during L-dopa production. The address for the corresponding author was captured as affiliation for all authors. Please check if appropriate. Biomac(2017), doi:10.1016/j.ijbiomac.2018.03.185

New insight into the allosteric effect of L-tyrosine on mushroom tyrosinase during L-dopa production

Sorour Hassani[a], Behzad Gharechaei[b], Somayeh Nikfard[a], Mostafa Fazli[b], Nematollah Gheibi[c], Renaud Hardré[d], Raymond L. Legge[e], Kamahldin Haghbeen[a*]

[a] National Institute for Genetic Engineering and Biotechnology, P.O. Box:14965-161, Tehran, Iran

[b] Department of Chemistry, Faculty of Science, Semnan University, Semnan, Iran

[c] Cellular and Molecular Research Center, Qazvin University of Medical Sciences, Qazvin, P.O. Box: 34199-15315, Iran

[d] Aix Marseille Univ, CNRS, Centrale Marseille, iSm2, Marseille, France

[e] Department of Chemical Engineering, University of Waterloo, 200 University Ave. W., Waterloo, ON, N2L 3G1, Canada

Corresponding authors: K. Haghbeen (Kamahl@nigeb.ac.ir), Phone: +98 21 44787372

Abbreviations: L-tyrosine (LTy)**,** mushroom tyrosinase (MT), 4-[(4-Methylphenyl) azo]-phenol (MePAPh)**,** phthalic acid (PA), cinnamic acid (CA)**,** *Bacillus megaterium* tyrosinase (BmT), Molecular Dynamic (MD), AutoDock Tools (ADT)

ABSTRACT

Kinetics studies of L-tyrosine (LTy) ortho-hydroxylation by mushroom tyrosinase (MT) confirmed that MT was severely, but not completely, inhibited at higher concentrations of LTy. Despite the availability of the crystal structure reports, no allosteric site has been identified on MT. To examine the assumption that a non-specific binding site works as a regulatory site, docking simulations were run for the second molecule of L-tyrosine (LTy_2) on the complexes of the first L-tyrosine molecule (LTy_1) with the heavy chain (H) of MT (LTy_1/HMT) and its dimer with the light chain (Ty_1/LHMT). In both, LTy_2 occupied a non-specific binding site (MTPc). MD simulations revealed LTy_2/HMT/LTy_1 and LTy_2/LHMT/LTy_1 were stable. Binding free-energy analysis supported the formation of LTy_2/HMT/LTy_1 and LTy_2/LHMT/LTy_1 at higher concentrations of LTy and disclosed the importance of ΔE_{elec} and ΔG_{polar} during binding of LTy_2 to MTPc. Upon LTy_2 binding to MTPc, the Cu-Cu distance remained unchanged while the spatial position of LTy_1 in the active site (MTPa) changed so that it would not be able to participate in ortho-hydroxylation. This study suggests a tuning role for L chain during binding of the ligands to MTPa and MTPc. Given these results, a plausible mechanism was proposed for the MT substrate inhibition.

Keywords: substrate inhibition, regulatory site, non-specific binding site

1. Introduction

Although there is evidence indicating association of tyrosinase (EC 1.14.18.1) with neurodegenerative diseases through oxidation of dopamine [1], this cuproenzyme is largely recognized for its key role in melanin production [2]; a process initiated by ortho-hydroxylation of L-tyrosine (LTy) by tyrosinase (Fig. 1). The product of this step, L-dopa, is not released from the active site but is further oxidized by tyrosinase to dopa-quinone. Since ortho-quinones are reactive molecules, they easily participate in intra- and intermolecular reactions which finally result in formation of bio-macromolecules known as melanin [3].

Tyrosinase undergoes substrate inhibition in the presence of LTy [4,5] which is likely necessary to control melanin production. However, during *in vitro* production of L-dopa, substrate inhibition hinders progress of the reaction at higher concentrations of LTy and limits the yield during biotransformation [6]. Despite structural differences between the human tyrosinase and MT [7], most of the kinetic studies have been conducted on mushroom tyrosinase (MT) due to the difficulties of working with human tyrosinase as well as the behavior similarities between MT and mammalian tyrosinase [8,9]. Although the controlling effect of LTy on tyrosinase and melanocytes is among the important issues of the current melanogenesis research [10], there is a lack of comprehensive report about the homotropic effect of LTy on MT.

MT is an asymmetric tetramer, H_2L_2, with an average molecular weight of 120 kDa. Each heavier subunit of active MT (HMT) is about 43 kDa and carries a binuclear copper active site, while the L subunit of MT (LMT) lacks an active site [11]. The pocket of MT active site (MTPa) is accessible through a cavity in the surface of HMT which is not occluded by LMT or by loops of the side chains of HMT [12].

Kinetics studies revealed cooperativity in both the mono-oxygenase (cresolase) and oxidase (catecholase) activities of MT [13]. The patterns of cooperativity were not simple as they

were dependent on both the structure and concentration of the substrate. For instance; in the presence of *p*-coumaric acid, MT showed negative cooperativity at concentrations lower than 10 µM (Hill constant of 0.76) and positive cooperativity at concentrations greater than 20 µM (Hill constant of 1.08). When caffeic acid was the substrate, MT showed only positive cooperativity [13].

The unusual cooperativity in MT influences the inhibition studies. In many cases, the inhibition results follow mixed or non-competitive modes [14,15]. Dual-response of MT to a modulator has also been reported [16,17]. For instance; when 4-[(4-Methylphenyl) azo]-phenol (MePAPh) was the substrate, MT was activated by ethyl xanthate at concentrations lower than 11.5 µM and inhibited at concentrations higher than 20 µM [16]. Similar results were obtained from the examination of aurone flavonoids effects on MT [18]. All these observations led in proposing the existence of a modulatory site on MT [19,20]. However, MT crystallographic reports (PDB ID: 2Y9W), even in the presence of an inhibitor (PDB: 2Y9X), did not offer any evidence for this assumption [12].

In our recent publication, searching for non-specific binding sites on MT, we showed how each of phthalic acid (PA) and cinnamic acid (CA), as two modulators with different structures, could form a ternary complex of substrate/MT/modulator [21]. The non-specific binding sites for PA and CA were named MTPb and MTPc, respectively. We demonstrated that the modulators could reach the active site through channels which connected the MTPb and MTPc to MTPa [21]. Here we explain the homotropic effect of LTy by revisiting substrate inhibition of MT during L-dopa production. Then, through looking at possible binding sites for LTy on MT and in view of the impact of L chain on the binding of LTy, we present a possible mechanism for the substrate inhibition.

2. Materials and methods

MT was prepared as previously described [22]. LTy was purchased from Merck (Darmstadt, Germany). Other chemicals were taken from the authentic samples. Double distilled water was used for making phosphate buffer solution (PBS). Spectrophotometric measurements were carried out in the conventional quartz cells (4 mL) using Analytik, Specord 210 (Jenna, Germany) spectrophotometer.

2.1. Enzymatic kinetics studies

All the enzymatic reactions were performed in PBS (50 mM, pH 6.8) in a total volume of 3 mL at 20±1 $^{\circ}$C. Fresh stock solution of MT was prepared for each set of measurements. Cresolase activity of MT in the presence of various concentrations of LTy was measured via monitoring accumulation of the chromophoric intermediates, mainly dopachrome at λ_{max}= 475 nm (ε = 3600 $M^{-1}cm^{-1}$) [23]. All the presented results are the averages of, at least, five measurements.

2.2. Computational methods

2.2.1. Docking simulations

Docking of LTy into the MT structure was performed using AutoDock Vina software [24]. AutoDock Tools 4.2.5.1 program (ADT) was used for preparing all the input files. A detailed analysis of the residues involved in the interactions between the ligand and the protein was conducted with UCSF Chimera 1.10.2 [25].

2.2.2. Focused docking into HMT

Crystal structure of native MT (PDB ID: 2Y9W) was derived from RCSB Protein Data Bank [12]. Water molecules and the heteroatoms (including the ligands) were removed and polar hydrogens were added to the receptor by ADT program [26]. Partial atomic charges were assigned by Kollman-united charges method. The original structure of LTy (CID: 6057) was derived from NCBI PubChem Compound Database. The Gasteiger charge was assigned to the ligand using ADT program. Docking simulation of LTy into HMT was carried out in the active site coordinates. The best pose with favorable binding free energy was selected as the initial structure in the MD simulations.

2.2.3. Blind docking into HMT

To search for an extra possible binding site on HMT, blind docking of the second molecule of tyrosine (LTy_2) on the complex of HMT and the first molecule of tyrosine (HMT/LTy_1) was investigated. The simulation was performed to the whole surface of the complex with the docking parameters of; grid size (x = 58.96, y = 55.78, z = 62.60 Å), grid center (x = 2.32, y = 29.33, z = 85 Å), exhaustiveness = 1000 and num_modes=100. The default settings were maintained for the other parameters. The best docking pose was then subjected to MD simulations.

2.2.4. Blind docking into the LH dimer

Docking simulation was also carried out on the LH dimer while LTy_1 had already occupied MTPa. The blind docking of LTy_2 was performed to the whole surface of LMT/HMT/LTy_1 complex by setting the grid size to (x = 67.32, y = 69.63, z = 81.67 Å), the grid center dimensions to (x = 18.56, y = 46.20, z = 40.55 Å), exhaustiveness = 1000 and num_modes = 100. The best resulting coordinates of the docked complex was subjected to MD run.

2.2.5. MD simulations

HMT/LTy_1, $LTy_1/HMT/LTy_2$, $LHMT/LTy_1$ and $LTy_1/LHMT/LTy_2$ complexes were subjected to MD simulations for validation of the docking results. The MD runs were carried out in the NPT ensemble (50 ns) for each system. Details of the MD experiments have been presented in the Supplementary document.

2.3. Binding Free Energy

The free energy of binding of LTy_1 and LTy_2 to MT was evaluated using Molecular Mechanics Poisson-Boltzmann Surface Area (MM-PBSA) method. The energetic terms were calculated for the equilibrated structures extracted at every 100ps of the stable intervals from the relevant 50ns MD trajectories by the equations explained in the Supplementary document.

3. Results and discussion

3.1. Kinetics of substrate inhibition of MT

During mono-oxygenase activity of MT in the presence of LTy, substrate inhibition was observed at a substrate concentration higher than 0.53 mM (Fig. 2A). Based on rapid equilibrium assumption, the general model illustrated in Scheme 1 is used to explain various types of inhibition including substrate inhibition [27]. In this model, the modulator which can be a second molecule of the substrate (S_2) is able to bind to a non-catalytic site prior and after binding of the first substrate molecule (S_1) to the catalytic site [27,28].

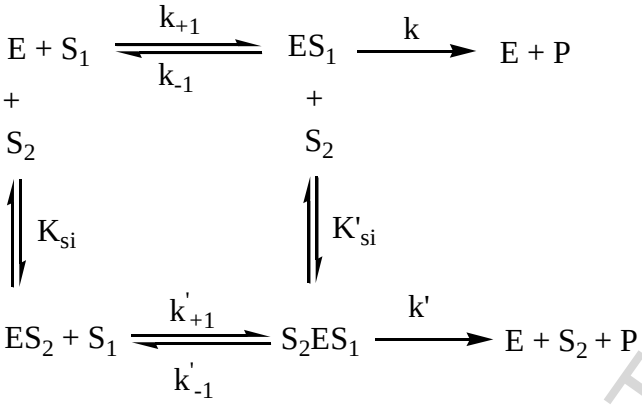

Scheme 1: General model for mechanism of substrate inhibition

K_{si} and K'_{si} are the dissociation constants of ES_2 and S_2ES_1 complexes while k and k' are the rate constants. Considering the assumptions that K_m is essentially the dissociation constant of ES complex ($K_m = k_{-1}/k_{+1}$) and the breakdown of ES_1 to E and P is the bottleneck of the model, the overall rate is obtained from the following equation [28]:

$$v = \frac{V_{max}(1+[S]/K'_{si}\times k'/k)\times[S]}{[S](1+[S]/K'_{si})+K_m(1+S/K_{si})} \qquad \textbf{[1]}$$

In non-competitive inhibition, the ternary complex of substrate/enzyme/inhibitor is a dead-end one. This would happen for the illustrated model if k′ was zero [28,29]. In uncompetitive inhibition model, the inhibitor can bind to the enzyme only after formation of ES complex. This happens for the illustrated model when $K_{si} = \infty$. In fact, most enzymologists explain substrate inhibition by the model of uncompetitive inhibition because the active site pocket usually offers the most favorable binding pose to the first molecule of the substrate [30]. In this case, equation 1 is simplified to the following equation:

$$v = \frac{V_{max}S}{K_m + S + (S^2/K'_{si})} \qquad \textbf{[2]}$$

In which:

$$K'_{si} = \frac{[ES_1][S_2]}{[S_2ES_1]} \qquad \textbf{[3]}$$

As seen in Fig. 2A, the experimental data for the mono-oxygenase activity of MT in the presence of LTy has a good visual fit to equation 2 [29], similar to what was reported for the substrate inhibition of cytochrome P450 in the presence of benzyloxyresorufin [31]. The inflexion point of the curve gives S_{max} *i.e*; the substrate concentration at which the reaction proceeds at its highest possible velocity (v_m).

$$S_{max} = \sqrt{K_m . K'_{si}} \quad \textbf{[4]}$$

The double-reciprocal form of equation 2 discriminates between uncompetitive and substrate inhibition as it produces straight line for the former and hyperbola for the latter case (Fig. 2B). Although it is possible to obtain the kinetic parameters of the substrate inhibition of MT by drawing the asymptotes of the hyperbola of Fig. 2B [32], more precise information is obtained by using the logarithmic form of equation 2. In case of substrate inhibition, the plot of *v* versus log[S] produces a symmetric bell shape curve (Fig. 2C). Two symmetric points of S_1 and S_2 on the curve present the substrate concentrations at which the velocity is half of v_m. Accordingly [33]:

$$K'_{si} = S_1 + S_2 - 4S_{max} \quad \textbf{[5]}$$

$$K_m = \frac{(S_{max})^2}{K'_{si}} \quad \textbf{[6]}$$

$$V_{max} = v_m \left[1 + 2\left(\frac{K_m}{K'_{si}}\right)^{1/2} \right] \quad \textbf{[7]}$$

Using these equations, kinetic parameters of V_{max} = 0.011 mM min^{-1}, K_m = 0.4 mM, and K'_{si} = 0.52 mM were obtained for the substrate inhibition ($K_{si} = \infty$) of MT by LTy. This data indicates lower affinity of MT/LTy_1 for LTy_2 than MT for LTy_1.

From the fitted hyperbola (illustrated in Fig. 2A), it is rather difficult to find whether the enzyme was completely inhibited or partially. The asymptote of the hyperbola is sensitive to K'_{si}. When $K'_{si}=\infty$, the hyperbola becomes a normal Michaelis-Menten curve but once the K'_{si}

value decreases, the asymptotes of the hyperbola descends [29]. This may become misleading at higher concentrations of the substrate. Through rearranging equation 1, Yoshino and his colleagues obtained the following equation [34]:

$$\frac{v}{V_{max}-v} = \frac{K'_{si}}{1-(k'/k)} \cdot \frac{1}{S} + \frac{(k'/k)}{1-(k'/k)} \qquad \textbf{(8)}$$

Accordingly, a plot of v/ (V_{max}-v) versus 1/[S] produces a line that passes through the origin when the substrate inhibition is complete, otherwise the line intersects the vertical axis at a point equal to (k'/k)/(1- k'/k) ratio [34]. Consequently, the kinetics data of MT produced the plot shown in Fig. 2D with k'/k value of 0.18. This means that MT was strongly, but not completely, inhibited at higher concentrations of LTy.

3.2. Docking studies

3.2.1. Blind and focused docking of LTy_1 into HMT

Results of the blind docking of LTy_1 into HMT (2Y9W) were ranked with respect to the binding affinity. As anticipated, LTy_1 achieved the most stable binding pose when it was in MTPa. A focused docking of LTy_1 on a space restricted to the active site area confirmed the binding pose of LTy_1 in MTPa (Fig. 3A) with the lowest binding energy of -6.4 kcal mol^{-1}. Similar to what was observed for LTy bound to *Bacillus megaterium* tyrosinase (BmT, PDB ID: 4P6S) [35], the hydroxyl group of LTy_1 was directed toward CuA (an equivalent position to ZnA in BmT) in MTPa (Fig. 3B). The ligand orientation in MTPa is assumingly resulted from the steric interactions of LTy_1 with His61, His85, His263, Val283, and stabilized through weak van der Waals interactions with Phe264, Phe292 and two hydrogen bonds (H-bonds) with Asn260 (3.13 Å), and Gly281 (2.16 Å) (Fig. S1A; Supplementary Material).

3.2.2. Blind docking of LTy_2 into HMT/LTy_1 complex

To explore for extra potential binding sites on HMT, a blind docking was performed for LTy_2 into HMT while MTPa was occupied by LTy_1. The simulation was run on the entire surface of HMT/LTy_1 complex. All the generated binding poses for LTy_2 were located in MTPc (Fig. 3C), the identified pocket for binding of CA to tropolone-bound MT (2Y9X) [21], with average binding energy of -5.7 kcal mol^{-1}. Analysis of LTy_2 binding mode reveals the importance of H-bonds in stabilizing the ligand pose in MTPc as there are four H-bonds between LTy_2 and Gln307 (2.10 Å), Asp312 (2.45 Å), Val313 (2.60 Å) and Glu356 (2.95 Å), (Fig. S1B), while there is only one possible π-π interaction with Trp358. Interestingly, the phenolic ring of LTy_2 plays no role in the H-bonds. In fact, the spatial orientation of the phenolic moiety of LTy_2 is almost toward the same direction of the aromatic ring of CA in MTPc, (Fig. S2A), [21].

3.2.3. Analysis of blind docking into LH dimer

L chain of MT is a non-immunogenic protein with structural homology close to the lectin family. The protein is encoded by the orf239342 gene, located in the same cluster with the tyrosinase gene in the mushroom chromosome. However, no specific biological activity has so far been reported for this protein [36]. In contrast to ORF378 which is essential for the activity of *Streptomyces castaneoglobisporus* tyrosinase [37], HMT shows activity in the absence of LMT [12]. LMT faces to HMT at a place far from the MTPa opening and covers about 800 $Å^2$ of the HMT surface where the interactions between these chains stabilize the structure of LH dimer [12].

To examine if there is any potential binding site for LTy_2 on LMT, a blind docking was first performed for LTy_1 on the entire surface of LH dimer. LTy_1 occupied MTPa in a binding pose similar to what was illustrated in Fig. 3A. Then, a blind docking was performed for

LTy_2 on the entire surface of LH dimer while LTy_1 was in MTPa. The simulation results suggested two potential binding sites; both on HMT. 80% of the suggested poses for LTy_2 were in MTPc and 20% of them were in a different pocket, named MTPd (Fig. 3D), with the average binding energy of -5.5 and -5.37 kcal mol^{-1}, respectively. These outcomes rule out the possibility of direct role of L chain as the host of a binding site for any LTy molecules. Concomitantly, these results indicate that addition of L chain to HMT creates some conformational changes which influence its affinity for LTy_2 while MTPc still remains as the main binding site for LTy_2.

3.3. Characterization of the binding modes in Molecular Dynamic (MD) simulation

3.3.1. HMT/LTy_1 and $LTy_2/HMT/LTy_1$

A 50 ns MD simulation was performed for each of the stable binding modes of HMT/LTy_1 and $LTy_2/HMT/LTy_1$. The plots of RMSD versus time, Fig. 4A, reveal that both systems reached the equilibrium state very fast and their protein backbones showed insignificant deviations over the rest of the simulation time. This means that the LTy_2 pose in MTPc did not threaten the stability of HMT/LTy_1 and the new complex of $LTy_2/HMT/LTy_1$ was as stable as HMT/LTy_1. The Radius of gyration (Rg) plots, Fig. 4B, also suggest good conformational stability for both systems as the average Rg of both complexes fluctuates around a low and nearly constant value, about 2.05 nm, without showing any substantial drift. These results indicate that MT does not experience significant conformational changes after binding the first, and even the second, molecule of LTy.

Reviewing RMSD plots of the ligands, Fig. 4C, reveals some minor discrepancies between LTy_1 and LTy_2 equilibrium state despite the overall stability of both ligands in their binding poses. LTy_2 reached equilibrium later than LTy_1 and experienced more oscillations during the simulation time. This is in agreement with the obtained binding energies of -6.4 and -5.7 kcal

mol^{-1} for HMT/LTy_1 and $LTy_2/HMT/LTy_1$, respectively. This difference can be ascribed to the interaction LTy_1 hydroxyl group with CuA and stabilizing interactions of its body with the surrounding residues in MTPa.

3.3.2. $LHMT/LTy_1$ and $LTy_1/LHMT/LTy_2$

To examine the effect of L chain on the binding modes of LTy_1 and LTy_2, the complex of $LTy_1/LHMT/LTy_2$ was also subjected to similar MD simulation. The complex reached equilibrium after 10 ns (green plot in Fig. 4A). Although its protein backbone showed more fluctuations as compared with that of $LTy_1/HMT/LTy_2$, it remained stable to the end of simulation. The Rg plot, Fig. 4B, illustrates that the protein skeleton of $LTy_1/LHMT/LTy_2$ maintained a stable folding around a relatively steady value of Rg, 2.58 nm. RMSD plots of the ligands reveal a little improvement in the stability of LTy_1 and LTy_2 in $LTy_1/LHMT/LTy_2$ (Fig. 4D) as compared with $LTy_1/HMT/LTy_2$, Fig. 4C. All the MD simulation results confirm the stability of the examined complexes and indicate that the addition of LTy_2 to MT is not accompanied by large conformational changes.

3.4. Analysis of the binding free energies

Thermodynamic data which is obtained from docking simulation relies on a single bound conformation while such information from MM-PBSA is generated by conformational sampling of the molecules involved in the binding during the MD simulation. Hence, the converged results of the ensemble express the thermodynamic averages of the involved molecules [38]. Inspecting the $\Delta G_{binding}$ values obtained from MM-PBSA method, Table 1, confirms lower affinity of MTPc for LTy_2 as compared with the affinity of MTPa for LTy_1. This explains why the substrate inhibition of MT happens at higher concentrations of LTy. This data also shows that the addition of L chain has reduced the affinities of both sites of

HMT for LTy molecules. This modifying effect of L chain may be meaningful from a controlling point of view.

The solvation energy data disfavors formation of any complexes of MT and LTy, but it is outweighed by favorable molecular mechanics energy contribution in the $\Delta G_{binding}$. Nonetheless, the share of the solvation free energy components deserves more attention. Although the values of the nonpolar components are about -2.5 kcal mol^{-1} for the examined complexes, ΔG_{polar} has increased 60 and 80% in the complexes of LTy_2 with HMT/LTy_1 and LHMT/LTy_1, respectively, as compared with the ΔG_{polar} of the LTy_1 binding with these complexes, Table 1. This result discloses that there is a substantial energy penalty for moving the polar parts of LTy_2 out of water and into the binding site [38]. In contrast to MTPa, MTPc is mainly constructed by hydrophilic residues, Fig. 3C. Consequently, sequestering water molecules away from these residues is an energy consuming step. However, this positive ΔG is largely compensated by favorable electrostatic interactions of LTy_2 at the ligand-protein interfaces in MTPc. This explains why ΔE_{elec} for the LTy_2 interactions are larger than 200% as compared with those of LTy_1 interactions, Table 1. This large gap between the ΔE_{elec} values is of interest as it sheds more light on the role of L chain in MT when the corresponding values of LTy_1 and LTy_2 in LTy_1/LHMT/LTy_2 are inspected. The difference goes beyond 300%. Apparently, the addition of L chain to the system has halved the electrostatic interactions of LTy_1 with the active site residues.

3.5. Geometric parameters of MTPa and MTPc

After LTy_2 entrance into MTPc, productivity of MT/LTy_1 is decreased. This means that following the LTy_2 binding to MT, some conformational changes happen which affect the binding of LTy_1 to MTPa, so that the ortho-hydroxylation of LTy_1 does not proceed at the expected rate. To see how the conformational changes are translated into the negative

homotropic effect on the active site, geometric parameters of MTPa in the complexes of HMT/LTy_1, LHMT/LTy_1, LTy_2/HMT/LTy_1, and LTy_1/LHMT/LTy_2 at the end of the MD simulations were extracted (Table 2) and examined.

3.5.1. Copper-copper distances

Cu-Cu distance plays a pivotal role in the catalytic activities of cuproproteins Type 3. The binding of molecular oxygen to deoxy form of these proteins usually shortens the Cu-Cu distance [39]. In arthropods hemocyanins, the changes in the Cu-Cu distance trigger large conformational changes which lead to cooperative oxygen binding [40]. In contrast, structural features of the core region of HMT protect the protein skeleton against large conformational changes following the changes in the Cu-Cu distance [39]. The data in Table 2 does not suggest any significant change in the Cu-Cu distance in the examined complexes. This indicates that the copper ions distance remained undisturbed not only after addition of L chain to the complexes of HMT/LTy_1 and LTy_2/HMT/LTy_1, but also after binding of LTy_2 to HMT/LTy_1 and LHMT/LTy_1.

3.5.2. Orientation of LTy_1 in MTPa

It seems that LTy_1 orientation in MTPa is more sensitive to the binding of the second ligand than the addition of L chain (Table 2). Comparing the data of HMT/LTy_1 and LHMT/LTy_1 discloses little changes in the geometric parameters of LTy_1 in the active sites. In contrast, binding of LTy_2 to HMT/LTy_1 causes a stretch of 0.2 Å in the PhO-Cu bond accompanied by a large tilt in the plane of the aromatic ring of LTy_1 (Fig. 5A). This change in the aromatic plane increases the distances of C_α^{L} and C_α^{U} (see Fig. 3A) from CuA (about 0.4 and 0.3 A, respectively) in LTy_2/LHMT/LTy_1, Table 2. This, in turn, assumingly decreases the efficiency of the ortho-hydroxylation by Cu_2O_2 on the aromatic ring. These results indicate

that the negative homotropic effect of LTy_2 is mainly exerted through the changes in the LTy_1 orientation in MTPa rather than the changes in the Cu-Cu distance.

3.5.3. Orientation of LTy_2 in MTPc

In Fig. 3C, it was shown that LTy_2 was surrounded by a net of H-bonds which gave it an orientation similar to what was observed for CA (Fig. S2A). Addition of L chain did neither block MTPc nor changed the preferred binding site for LTy_2. Nonetheless, reviewing the binding pose of LTy_2 in MTPc of LTy_2/LHMT/LTy_1 reveals that the addition of L chain to HMT has reduced the number of H-bonds to LTy_2, with Gln307 (1.84 Å) and Glu356 (2.22 Å), Fig. 5B. This, in turn, results in a change in the LTy_2 orientation in MPTc (Fig. S2B).

Given the fact that HMT shows activity by itself [11] and considering the results of Tables 1 and 2, it seems likely that the association of L chain helps MT establish a more persistent functional conformation through adjusting the electrostatic and hydrophobic interactions in MTPa and the non-specific binding site. This tuning effect of L chain may play a critical role in the communication of MT with its environment via the non-specific binding sites such as MTPc.

The MTPc pocket is located close to the interface zone of H-H in H_2L_2 [12]. Examination of the 3-D structures illustrated in Fig. 3C and 5B reveals that MTPc is constructed by the residues mainly located on a loop, illustrated in yellow color in Fig. 5B, which starts from Asn310, at the end of helix (α11) and reaches to Lys376 at the beginning of helix (α13) [12]. Glu356 (at the middle of the loop), and Gln307 [located on helix (α11)], are in direct contact with LTy_2. Helix (α11) is one the four central helices, which encompass the active site of MT by providing the copper ions with the coordinating histidines [41], and carries His296, Fig. 6A. It is assumed that, after the LTy_2 entrance into MTPc, these direct contacts provide a driving force for the movement of helix (α11) which reaches to His296, Fig. 6B.

Among the coordinating histidines of the copper ions in MT, 4 histidines (61, 94, 259, 263) have H-bonds from their Nδ1 atoms to the carbonyl oxygens of the protein skeleton and the thioether bond with Cys83 fixes the orientation of His85. In contrast, the imidazole ring of His296 is free to rotate, however, the orientation of His296 is protected through an indirect H-bond of its residue to the protein body [12]. In the view of the fact that there are some structural constraints which support relatively stable distance of the copper ions in MT, regardless of the possibility of accommodating alternative locations during different steps of the catalytic cycles for the coppers [42], it is assumed that the movement of helix (α11) triggers subtle changes in the orientation of His296 which is translated, through the net of H-bonds, to some fine conformational changes in the other coordinating histidines without changing the Cu-Cu distance, Fig. 6B. As a result of these changes, His85 and His61 exert a repelling force on the aromatic ring of LTy_1 in MTPa that pushes its C_α out of reach for hydroxylation. Based on the crystallography evidence, it has been proposed that the proper rotation of the aromatic plane of LTy, in its binding pose in MTPa, is necessary for ortho-hydroxylation. Any constraint which threatens this possibility would obstruct mono-phenolase activity [35].

4. Conclusions

Substrate inhibition renders an enzyme able to control its physiological functions but works as a barrier in biotransformation plans. Kinetics studies confirmed that MT is strongly, but not completely, inhibited at higher concentrations of LTy. Although the crystal structure and extensive works reports had not suggested any regulatory site on MT. Using computational methods, it was shown that a non-specific binding site works as a regulatory site through which the negative homotropic effect of LTy is exerted. Given these results, a plausible mechanism was proposed for the MT substrate inhibition. The non-specific binding site

locates on HMT and LMT assumingly plays a tuning role during binding of the ligands to the active site and the non-specific binding site.

Acknowledgements

We would like to thank Dr M. Sadeghi for his assistance in running the computational experiments. We also grateful of the financial support of the project by the Iran National Science Foundation (grant number: 93031596).

Conflict of interest

The authors declare that they have no conflicts of interest with the contents of this article.

Author contributions

K. Haghbeen conceived and designed research; S. Hassani, B. Gharechaei, S. Nikfard performed research; M. Fazli contributed new reagents/analytic tools; K. Haghbeen, S. Hassani, M. Fazli and N. Gheibi analyzed data; K. Haghbeen wrote the paper; R.L. Legge and R. Hardré reviewed manuscript and added comments. All authors reviewed the results and approved the final version of the manuscript.

REFERENCES

1. E. Herrero Hernández, Pigmentation genes link Parkinson's disease to melanoma, opening a window on both etiologies. *Med. Hypotheses* 72 (2009) 280–284.

2. T. Pillaiyar, M. Manickam, V. Namasivayam, Skin whitening agents: medicinal chemistry perspective of tyrosinase inhibitors *J. Enz. Inhib. Med. Chem.* 32(1) (2017) 403–425.

3. C. Olivares, F. Solano, New insights into the active site structure and catalytic mechanism of tyrosinase and its related proteins *Pigm. Cell Melanoma. Res.* 22 (2009) 750–760.

4. S. H. Pomerantz, The tyrosine hydroxylase activity of mammalian tyrosinase. *J. Biol. Chem.* 241 (1966) 161-168.

5. A. Sanchez-Ferrer, J. N. Rodriguez-Lopez, F. Garcia-Canovas, F. Garcia-Carmona, Tyrosinase: A comprehensive review of its mechanism. *Biochim. Biophys. Acta* 1247 (1995) 1–11.

6. M. Cieńska, K. Labus, M. Lewańczuk, T. Koźlecki, J. Liesiene, J. Bryjak, Effective L-tyrosine hydroxylation by native and immobilized tyrosinase. *PLoS ONE* 11(10) (2016) e0164213.

7. X. Lai, M. Soler-Lopez, H. J. Wichers, B.W. Dijkstra, Large-scale recombinant expression and purification of human tyrosinase suitable for structural studies. *PLoS ONE* 11(8) (2016) e0161697.

8. E. Baharav, E. Baharav, O. Merimski, Y. Shoenfeld, R. Zigelman, B. Gilbrud, G. Yecheskel, P. Youinou, P. Fishman, Tyrosinase as an autoantigen in patients with vitiligo. *Clin. Exp. Immunol.* 105(1) (1996) 84-88.

9. K. U. Zaidi, S. Ayesha, A. Sharique, Purification and Characterization of Melanogenic Enzyme Tyrosinase from Button Mushroom. *Enz. Res.* (2014) Article ID 120739, doi.org/10.1155/2014/120739.

10. A. Slominski, M. Zmijewski, J. Pawelek, L-tyrosine and L-DOPA as hormone-like regulators of melanocytes functions. *Pigm. Cell Melanoma Res.* 25(1) (2012) 14–27.

11. S. G. Mauracher, C. Molitor, C. Michael, M. Kragl, A. Rizzi, A. Rompel, High level protein-purification allows the unambiguous polypeptide determination of latent isoform PPO4 of mushroom tyrosinase. *Phytochemistry* 99 (2014) 14-25.

12. W. T. Ismaya, H. J. Rozeboom, A. Weijn, J. J. Mes, F. Fusetti, H. J. Wichers, B. W. Dijkstra, Crystal structure of Agaricus bisporus mushroom tyrosinase: Identity of the tetramer subunits and interaction with tropolone. *J. Biochem.* 50 (2011) 5477–5486.

13. K. Haghbeen, M. Babeli-Khalili, F. Sqeid-Nematpour, N. Gheibi, M. Fazli, M. Alijaninzadeh, S. Zolghadri-Jahromi, R. Sariri, Surveying allosteric cooperativity and cooperative inhibition in mushroom tyrosinase. *J. Food Biochem.* 34 (2010) 308-328.

14. N. Gheibi, N. Taherkhani, A. Ahmadi, K. Haghbeen, D. Ilghari, Characterization of inhibitory effects of the potential therapeutic inhibitors, benzoic acid and pyridine derivatives, on the monophenolase and diphenolase activities of tyrosinase. *Iran J. Basic. Med. Sci.* 18(2) (2015) 122–129.

15. T. S. Chang, An Updated Review of Tyrosinase Inhibitors. *Int. J. Mol. Sci.* 10 (2009) 2440-2475.

16. M. Alijanianzadeh, A. A. Saboury, H. Mansuri-Torshizi, K. Haghbeen, A. A. Moosavi-movahedi, The inhibitory effect of some new synthesized xanthates on mushroom tyrosinase activities. *J. Enzyme Inhib. Med. Chem.* 22(2) (2007) 239–246.

17. N. Gheibi, A. A. Saboury, K. Haghbeen, F. Rajaei, A. A. Pahlevan, Dual effects of aliphatic carboxylic acids on cresolase and catecholase reactions of mushroom tyrosinase. *J. Enz. Inhib. Med. Chem.* 24 (2009) 1076-1081.

18. E. Marková, M. Kotik, A. Křenková, P. Man, R. Haudecoeur, A. Boumendjel, R. Hardré, Y. Mekmouche, E. Courvoisier-Dezord, M. Réglier, L. Martínková, Recombinant Tyrosinase

from *Polyporus arcularius*: Overproduction in Escherichia coli, Characterization, and Use in a Study of Aurones as Tyrosinase Effectors. *J. Agric. Food Chem.* 64(14) (2016) 2925–2931.

19. D. E. Wilcox, A.G. Porras, Y. T. Hwang, K. Lerch, M. E. Winkler, E. I. Solomon, Substrate analogue binding to the coupled binuclear Copper active site in tyrosinase. *J. Am. Chem. Soc.* 107 (1985) 4015-4027.

20. M. Lin, L. Ke, P. Han, L. Qiu, Q. Chen, H. Lin, Q. Wang, Inhibitory effects of p-alkylbenzoic acids on the activity of polyphenol oxidase from potato (*Solanum tuberosum*). *Food Chem.* 119 (2010) 660–663.

21. S. Hassani, K. Haghbeen, M. Fazli, Non-specific binding sites help to explain mixed inhibition in mushroom tyrosinase activities. *Eur. J. Med. Chem.* 122 (2016) 138-148.

22. K. Haghbeen, F. Rastgar-Jazii, A. A. Karkhane, S. H. Shareefi-Borojer, Purification of tyrosinase from edible mushroom. *Iran J. Biotechnol.* 2 (2004) 189-194.

23. A. Spada, S. Palavicini, E. Monzani, L. Bubacco, L. Casella, Trapping tyrosinase key active intermediate under turnover. *Dalton Trans.* 33 (2009) 6468-6471.

24. O. Trott, A. J. Olson, Autodock vina: Improving the speed and accuracy of docking with a new scoring function, efficient optimization and multithreading. *J. Comput. Chem.* 31 (2) (2010) 455-461.

25. E. F. Pettersen, T. D. Goddard, C. C. Huang, G. S. Couch, D. M. Greenblatt, E. C. Meng, T. E. Ferrin, UCSF Chimera a visualization system for exploratory research and analysis. *J. Comput. Chem.* 25(13) (2004)1605-1612.

26. G. M. Morris, G. M. Morris, R. Huey, W. Lindstrom, M. F. Sanner, R. K. Belew, D. S. Goodsell, A. J. Olson, Autodock4 and autodocktools4: Automated docking with selective receptor flexibility. *J. Comput. Chem.* 30 (16) (2009) 2785–2791.

27. M. Yoshino, A graphical method for determining inhibition parameters for partial and complete inhibitors. *Biochem. J.* 248 (1987) 815-820.

28. M. C. Reed, A. Lieb, H. F. Nijhout, The biological significance of substrate inhibition: A mechanism with diverse functions. *BioEssays* 32 (2010) 422–429.

29. M. Yoshino, K. Murakami, A graphical method for determining inhibition constants. *J. Enz. Inhib. Med. Chem.* 24(6) (2009) 1288–1290.

30. X. Y. Meng, H. X. Zhang, M. Mezei, M. Cui, Molecular docking: A powerful approach for structure-based drug discovery. *Curr. Comput. aid drug* 7(2) (2011) 146–157.

31. Y. Lin, P. Lu, C. Tang, Q. Mei, G. Sandig, A. D. Rodrigues, T. H. Rushmore, M. Shou, Substrate inhibition kinetics for cytochrome p450-catalyzed reactions. *Drug Metab. Dispos.* 29 (2001) 368–374.

32. W. W. Cleland, Substrate inhibition. *Meth. Enzymol.* 63 (1979) 500-513.

33. I. M. Verhamme, G.W.K. Van Dedem, A. R. Lauwers, Ionic-strength-dependent substrate inhibition of the lysis of *micrococcus luteus* by hen egg-white lysozyme. *Eur. J. Biochem.* 172 (1988) 615-620.

34. M. Yoshino, K. Murakami, Analysis of the substrate inhibition of complete and partial types. *Springer Plus* 4 (2015) 292.

35. M. Goldfeder, M. Kanteev, S. Isaschar-Ovdat, N. Adir, A. Fishman, Determination of tyrosinase substrate-binding modes reveals mechanistic differences between type-3 copper proteins. *Nat. Commun.* 5 (2014) 4505.

36. W. T. Ismaya, O. M. Tandrasasmita, S. Sundari, Diana, X. Lai, D. S. Retnoningrum, B. W. Dijkstra, R. R. Tjandrawinata, H. Rachmawati, The light subunit of mushroom *Agaricus bisporus* tyrosinase: its biological characteristics and implications. *Int. J. Biol. Macromol.* 102 (2017) 308-314.

37. Y. Matoba, T. Kumagai, A. Yamamoto, H. Yoshitsu, M. Sugiyama, Crystallographic evidence that the dinuclear copper center of tyrosinase is flexible during catalysis. *J. Biol. Chem.* 281 (2006) 8981-8990.

38. M. K. Gilson, H. X. Zhou, Calculation of protein-ligand binding affinities. *Annu. Rev. Biophys. Biomol. Struct*. 36 (2007) 21-42.

39. E. I. Solomon, D. E. Heppner, E. M. Johnston, J. W. Ginsbach, J. Cirera, M. Qayyum, M. T. Kieber-Emmons, C. H. Kjaergaard, R. G. Hadt, L. Tian, Copper active sites in biology. *Chem. Rev*. 114 (7) (2014) 3659−3853.

40. M. Perbandt, M. Perbandt, E. W. Guthöhrlein, W. Rypniewski, K. Idakieva, S. Stoeva, W. Voelter, N. Genov, C. Betzel, The structure of a functional unit from the wall of a gastropod hemocyanin offers a possible mechanism for cooperativity. *Biochemistry-US.* 42 (21) (2003) 6341-6346.

41. N. Fujieda, S. Yabuta, T. Ikeda, T. Oyama, N. Muraki§, G. Kurisu, S. Itoh, Crystal structures of copper-depleted and copper-bound fungal pro-tyrosinase *J. Biol. Chem.* 288 (30) (2013) 22128–22140.

42. J. Yoon, S. Satoshi Fujii, E. I. Solomon, Geometric and electronic structure differences between the type 3 copper sites of the multicopper oxidases and hemocyanin/tyrosinase. *Proc. Natl. Acad. Sci. USA* 106(16) (2009) 6585– 6590.

Legends

Figure 1. Oxidation of L-tyrosine by tyrosinase is the key step of melanogenesis.

Figure 2. A) Kinetics graph of mono-oxygenase activity of MT in the presence of various concentrations (0.1, 0.2, 0.4, 0.5, 1, 1.2, 1.5, 2, 4, 6, 8 mM) of LTy in PBS at pH 6.8 and 20 °C. **B)** Lineweaver-Burk and **C)** logarithmic plots of the kinetics data shown in Fig. 2A. **D)** The plot of equation 12. Dotted line was the theoretical curve and the solid line was drawn within the range of the substrate concentration.

Figure 3. Results of docking simulations; **A)** Binding pose of LTy in MTPa of HMT, **B)** The spatial orientation of LTy with regard of the copper ions and the coordinating histidines in MTPa of HMT, **C)** Binding pose of LTy_2 in MTPc in the LTy_1/HMT/LTy_2 complex, and **D)** Relative spatial positions of MTPc and MTPd with respect to MTPa in LHMT.

Figure 4. Results of the MD simulations as a function of the simulation time; **A)** RMSD plot of MT backbone in HMT/LTy_1 [red], LTy_2/HMT/LTy_1 [blue] and LTy_2/LHMT/LTy_1 complex [green], **B)** Radius of gyration (Rg) plot during for HMT/LTy_1 [red], LTy_2/HMT/LTy_1 [blue] and LTy_2/LHMT/LTy_1 [green] complex, **C)** RMSD plot of LTy_1 in MTPa in HMT/LTy_1 [orange], LTy_2/HMT/LTy_1 [pink], and LTy_2 in MTPc [blue] of LTy_2/HMT/LTy_1, and **D)** RMSD plot of the ligands in LTy_2/LHMT/LTy_1 complex: LTy_1 in MTPa [blue] and LTy_2 in MTPc [pink].

Figure 5. A) Overlaid poses of LTy_1 in LTy_1/HMT (orange coordinating histidines) and LTy_1/HMT/LTy_2 (purple coordinating histidines) in white and grey color, respectively. **B)** Binding pose of LTy_2 in MTPc in LTy_1/LHMT/LTy_2 complex.

Figure 6. A) Relative spatial position of LTy2 with respect to Gln307 and His296. **B)** Overlaid poses of LTy_1 in LTy_1/HMT (orange coordinating histidines) and LTy_1/HMT/LTy_2 (purple coordinating histidines) in white and grey color, respectively.

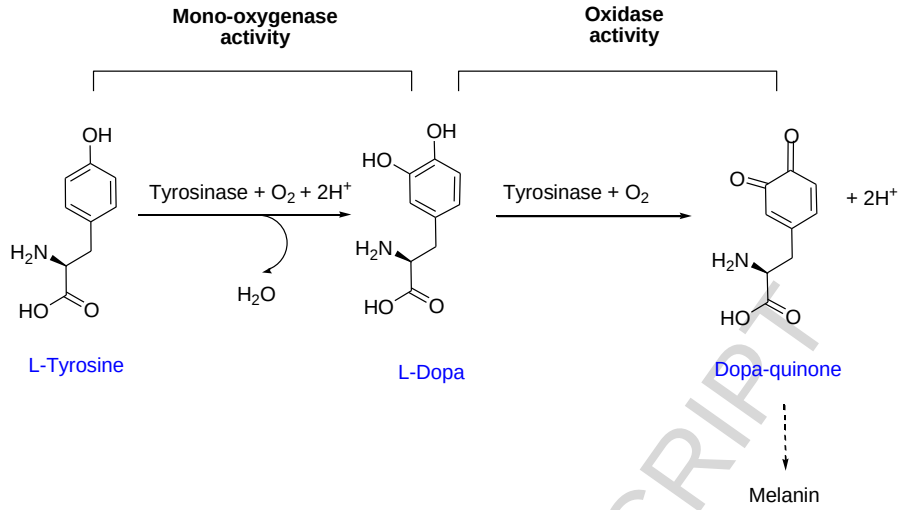

Figure 1.

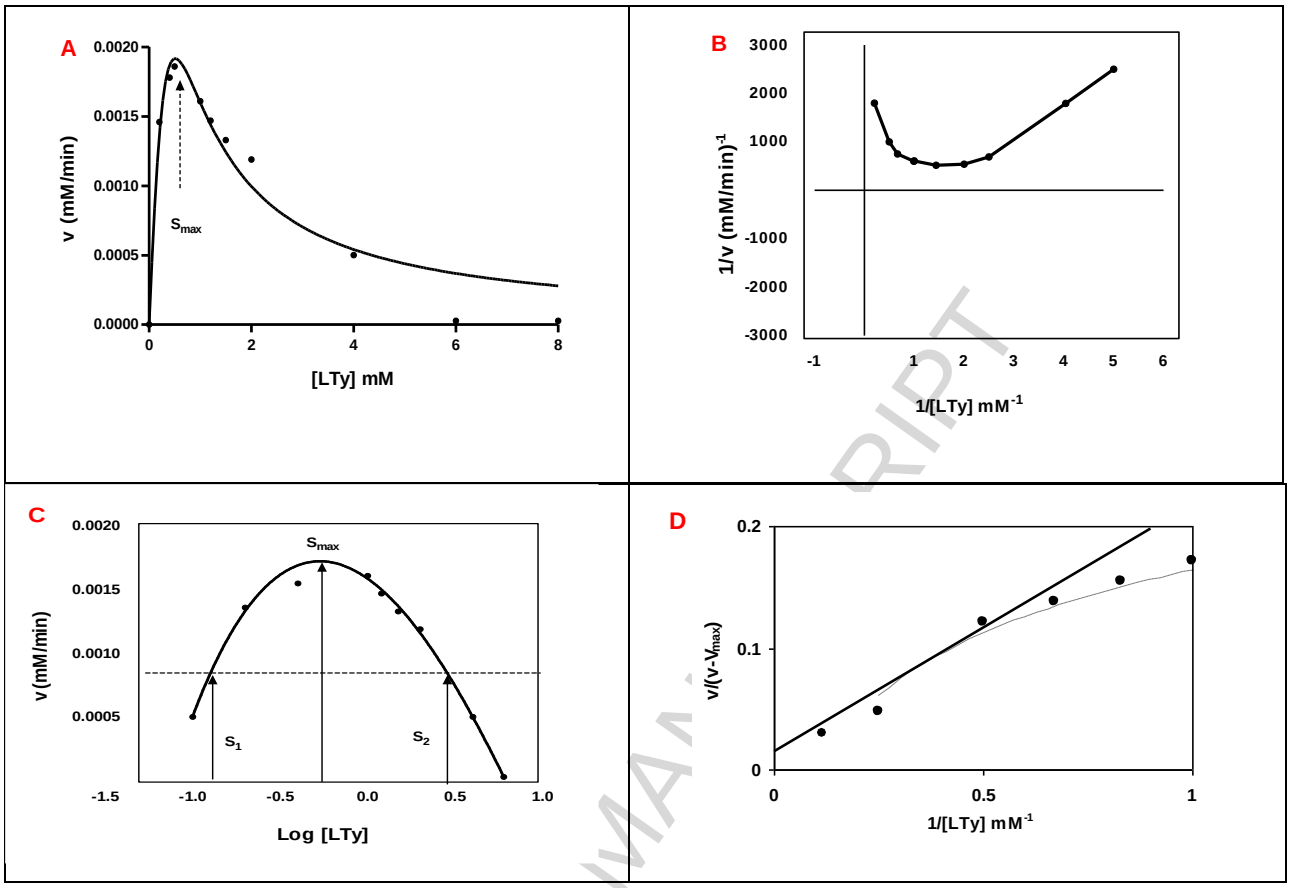

Figure 2.

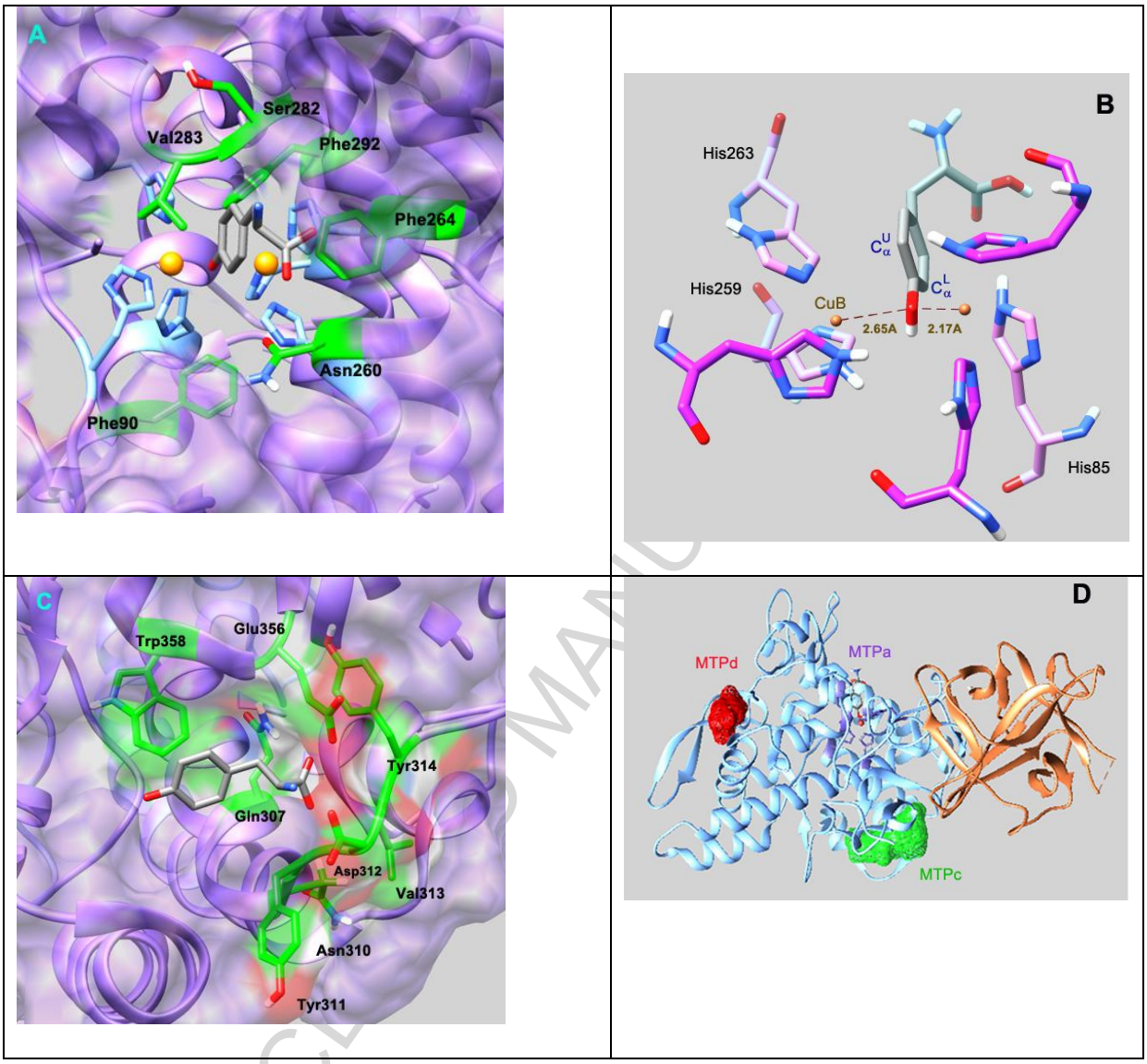

Figure 3.

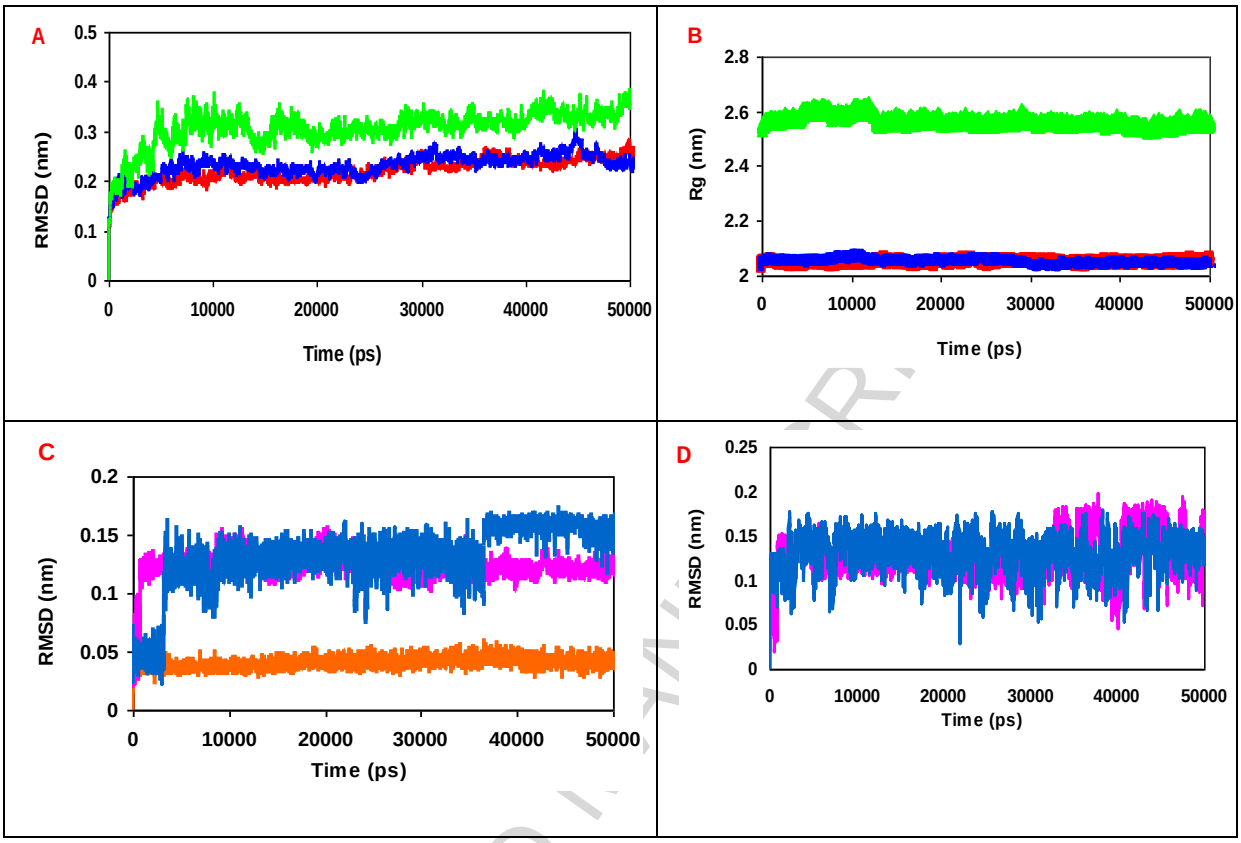

Figure 4.

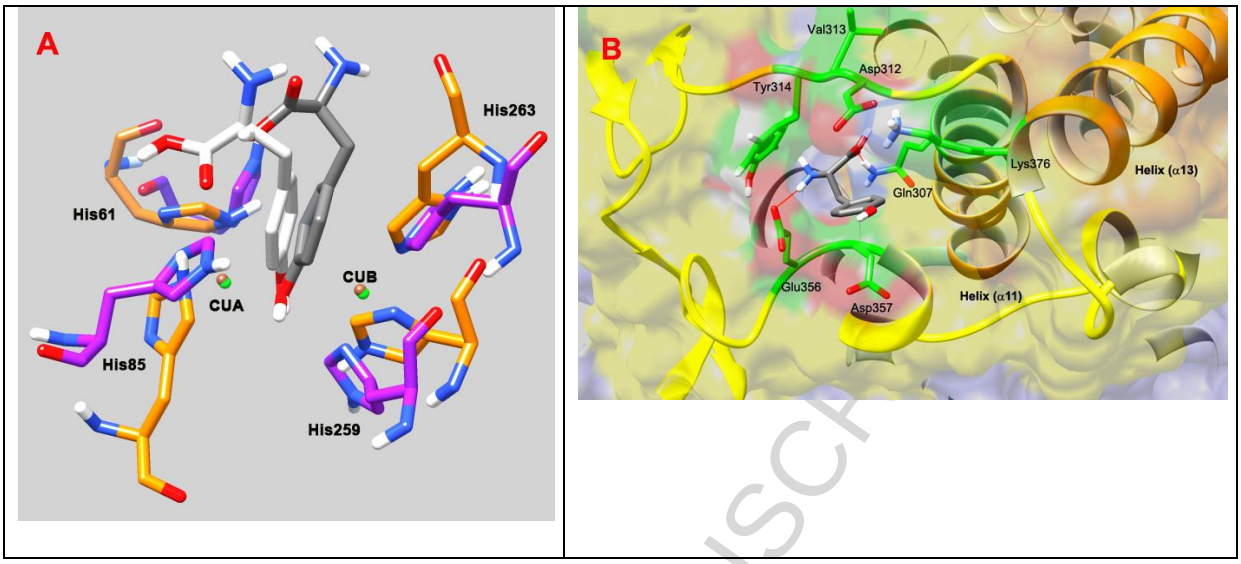

Figure 5.

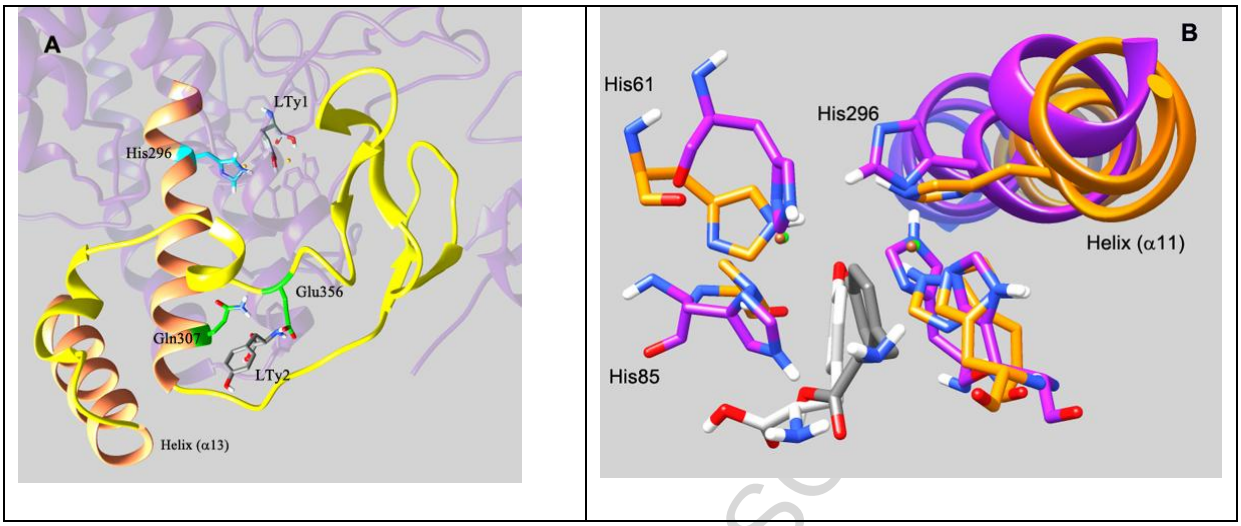

Figure 6.

Table 1. Analysis of the binding free energies of LTy in MTPa and MTPc pockets of the examined complexes

Examined Complexes	**ΔE_{vdw}***	**ΔE_{elec}**	**$\Delta G_{nonpolar}$**	**ΔG_{polar}**	**$\Delta G_{binding}$**
LTy_1 in MTPa in HMT/LTy_1	-20.78	-7.55	-2.57	27.50	-3.40
LTy_1 in MTPa in LTy_2/HMT/ LTy_1	-14.31	-11.76	-2.81	25.99	-2.89
LTy_2 in MTPc in LTy_2/HMT/ LTy_1	-15.91	-25.30	-2.60	41.72	-2.09
LTy_1 in MTPa in LTy_2/LHMT/ LTy_1	-15.77	-6.02	-2.24	21.98	-2.05
LTy_2 in MTPc in LTy_2/LHMT/ LTy_1	-15.70	-22.35	-2.69	39.39	-1.35

* ΔE_{vdw}, ΔE_{elec}, $\Delta G_{nonpolar}$ and ΔG_{polar} are components of binding energy including van der Waals and electrostatic components of molecular mechanic term and nonpolar and polar components of solvation energies, respectively. The unit of energy is kcal mol^{-1}.

Table 2. Geometric parameters of LTy_1 in MTPa of the examined complexes at the end of 50 ns MD simulations

Examined Complexes	CuA—CuB Å	CuA—O* Å	C_α^L—CuA Å	C_α^U—CuA Å	∠C_α^L-CuA- C_α^U	∠CuA-O-CuB
HMT/LTy_1	4.46	2.17	3.85	3.55	37.75	135.77
LHMT/LTy_1	4.47	2.18	3.80	3.60	36.95	135.55
LTy_2/HMT/LTy_1	4.45	2.4	4.29	3.35	34.08	126.09
LTy_2/LHMT/LTy_1	4.48	2.22	4.28	3.92	33.97	121.26

* "**O**" denotes oxygen of the phenolic hydroxyl group of LTy_1. $\mathbf{C_\alpha^L}$ and $\mathbf{C_\alpha^U}$ denote the α-carbons to the phenolic hydroxyl functional group of LTy_1 illustrated in Fig. 3B.

Highlights

- Comprehensive kinetics of substrate inhibition of mushroom tyrosinase (MT) by L-tyrosine (LTy) is presented.
- Computational studies indicate that a non-specific binding site helps MT to form the ternary complex of LTy_1/MT/LTy_2.
- The non-specific binding site locates on the heavy chain of MT.
- A plausible mechanism was proposed for the MT substrate inhibition.
- A tuning role for the light chain of MT during binding of the ligands was demonstrated.